A&A 403, 869–876 (2003)
DOI: 10.1051/0004-6361:20030395

Astronomy & Astrophysics

On the *XMM-Newton* spectra of soft X-ray selected QSOs

A. Akylas[1,2], I. Georgantopoulos[1], and X. Barcons[3]

[1] Institute of Astronomy & Astrophysics, National Observatory of Athens, Palaia Penteli, 15236 Athens, Greece
[2] Physics Department, University of Athens, Panepistimiopolis, Zografos, 15783 Athens, Greece
[3] Instituto de Fisica de Cantabria, CSIC-UC, 39905 Santander, Spain

Received 31 May 2002 / Accepted 11 March 2003

Abstract. We study the *XMM-Newton* spectra of a sample of 32 soft X-ray selected QSOs. Our goal is to check, using the spectra of moderate redshift ($z \sim 1.5$), faint ($f_{0.2-8\ \mathrm{keV}} > 5 \times 10^{-15}$ erg cm^{-2} s^{-1}) broad-line QSOs, previous claims for either significant intrinsic absorption or spectral hardening at high energies. We derive hardness ratios for all sources and furthermore we perform spectral fits for the 11 brighter sources. The majority of sources have steep spectra $\Gamma > 1.9$. We find a few QSOs with large amounts of intrinsic absorption, as high as $N_{\mathrm{H}} \sim 10^{23}$ cm^{-2}. We find no strong evidence for spectral hardening above 2 keV. The coadded QSO spectrum is well described by a single power-law with photon index of ~1.9, demonstrating that, on average, any effects of absorption are not important. This suggests that the discrepancy between the X-ray background and the (soft X-ray selected) QSO spectrum holds well at the faint fluxes probed here.

Key words. galaxies: active – quasars: general – X-rays: galaxies – X-rays: general

1. Introduction

In the last decade there has been a great progress in understanding the X-ray spectral properties of QSOs (see Mushotzky et al. 1993 for a review). *GINGA* (Lawson & Turner 1997) and *ASCA* (Reeves & Turner 2000) observations of nearby, bright QSOs (typically with flux $>10^{-12}$ erg s^{-1} cm^{-2}) in the 2–10 keV band have shown a power-law spectrum ($\Gamma \sim 1.9$) with no evidence for absorption above the Galactic value. At softer energies (0.1–2 keV) *ROSAT* observations show a much steeper spectrum ($\Gamma \sim 2.5$, Laor et al. 1997). This steepening is attributed to either an additional soft component at energies <0.5 keV or simply to calibration uncertainties between different instruments (Iwasawa et al. 1999). In any case, the bright QSO spectra in the 0.5–10 keV band are much steeper than the spectrum of the X-ray background (XRB) which has $\Gamma = 1.4$ (Gendreau et al. 1995; Miyaji et al. 1998; Vecchi et al. 1999). This spectral mismatch known as the spectral paradox suggested that QSOs cannot produce the bulk of the X-ray background.

However, the spectrum of a broad-line $L_\star$ QSO (those which contribute a significant fraction of the XRB) at large distances ($z \sim 1.5$) is largely unknown. Schartel et al. (1996), Blair et al. (2000) studied the co-added spectra of faint distant QSOs with *ROSAT*. They find an average spectrum of $\Gamma \sim 2.1-2.6$ flattening with increasing redshift. Pappa et al. (2001) studied the *ROSAT/ASCA* spectrum of 21 hard X-ray selected QSO. They find evidence for spectral curvature in the sense that the 2–10 keV *ASCA* spectrum has $\Gamma \sim 1.5$ while their *ROSAT* spectrum is steep $\Gamma \sim 2.2$. More recently, Barcons et al. (2002) found evidence for such a spectral curvature in the average QSO hardness ratio in their *XMM-Newton* SSC Medium Sensitivity survey. They find $\Gamma \sim 2$ and $\Gamma \sim 1.6$ at soft (0.5–4.5 keV) and hard (2–10 keV) energies respectively. Moreover, it becomes now evident that some QSOs present high amounts of obscuration (e.g. Fiore et al. 1999). The above results bear great significance as they may suggest that QSOs can contribute a larger fraction of the X-ray background than that usually predicted by the standard synthesis models (e.g. Comastri et al. 1995).

In this paper we exploit the large effective area and the extended passband of *XMM-Newton* in order to analyze the spectral properties of faint $f_{0.2-8\ \mathrm{keV}} > 5{\times}10^{-15}$ erg cm^{-2} s^{-1}($\Gamma = 2$) Broad-Line QSOs. In particular, we analyze the spectral properties of 32 soft X-ray selected, broad-line (type-I), QSOs in the Lockman Hole (Schmidt et al. 1998; Lehmann et al. 2001). These QSOs contribute a significant fraction (~50% in the 0.9–2 keV band) of the X-ray background intensity (Hasinger et al. 1993). Results on the *XMM-Newton* properties of all sources in the Lockman Hole have been presented by Hasinger et al. (2001) and Mainieri et al. (2002). Here instead, we put emphasis on testing for the presence of absorption or spectral flattening at high energies in the individual or co-added QSO spectra and the implications for the X-ray background.

2. The X-ray data

We use *XMM-Newton* data from the Lockman Hole Observation, centered on the sky position RA 10:52:43,

Send offprint requests to: I. Georgantopoulos,
e-mail: ig@astro.noa.gr

DEC +57:28:48 (J2000). In particular we use data from three *XMM-Newton* observations, (revolutions 70, 73 and 74) with total exposure time (on-time) of ∼120 ks. The astrometry offsets between the 3 revolutions above are within only a couple of arcsec and therefore they are not taken into account. We analyse the pipeline products using the *XMM-Newton* Science Analysis System (SAS v5.3). We deal only with data from the EPIC-PN camera because its sensitivity is significantly greater than that of MOS (Strüder et al. 2001). The EPIC-PN camera was operated in the standard full-frame mode. The pixel size corresponds to ∼4.1 arcsec. For on-axis point sources, a circle of radius ∼32 arcsec includes 90% of the 1.5 keV photons and 85% of the 5 keV photons. The Point–Spread–Function (PSF) does not strongly depend on the off-axis angle. For sources at 7 arcmin off-axis the above radius encircles almost the same percentage of soft and hard photons. The vignetting correction is ∼28% for 1.5 keV photons and ∼31% for 5 keV photons at 7 arcmin off-axis. The thin filter is used in all three observations. We constructed the event file using single and double events (patterns 0–4).

The signal-to-noise ratio of the sources becomes low at high energies due to the presence of a strong background Cu-Ka line at 8.1 keV. Therefore we have excluded from our analysis photons with energies >8 keV. A substantial fraction of the observations were also affected by high particle background with count rate up to several hundred per second, compared to a quiescent count rate of several counts per second. We locate flares by analyzing the full field-of-view (FOV) light curves. We reject all the time intervals with count rates, in the 0.2–8 keV band, higher than 10 cts/s. The remaining good time intervals give an exposure of ∼50 ks.

We extract four images in the following bands: 0.2–0.5, 0.5–2, 2–4.5 and 4.5–8 keV. Exposure maps, which account for vignetting, CCD gaps, bad columns, and bad pixels, are constructed for each band. We also extract background maps for each energy band. We use the EBOXDETECT task to search for sources in the four images simultaneously. We use a detection likelihood of 18. This corresponds to less than one spurious detection per image. The same routine was used to derive the hardness ratios.

We obtain the optical identifications of the detected sources from the *ROSAT* Ultra Deep Survey Optical Identification catalogue (Lehmann et al. 2001). We select all sources classified as type I QSOs by Lehmann et al. (2001) i.e. these with optical spectroscopic class a, b or c. There are 44 QSOs within the *XMM-Newton* FOV: 3 fall on CCD gaps or bad columns, 2 are not detected while 7 are not considered for spectral analysis as they are faint. The resulting sample contains 32 QSOs. Four of these are associated with radio sources in the sample of de Ruiter et al. (1997). Hereafter, we refer to these as the "radio-loud" QSOs, regardless of whether these follow the criterion $L(5\ \mathrm{GHz}) > 2.5\times10^{24}\ h_{100}^{-2}\ \mathrm{WHz}^{-1}$ (Kellermann et al. 1989). The sample covers a redshift range from 0.2 to 3.4, with a mean of $z \sim 1.5$. The lower and upper fluxes are 5.3×10^{-15} and 6.5×10^{-13} ergs s^{-1} cm^{-2} respectively in the 0.2–8 keV band, assuming a power-law model with $\Gamma = 2$.

3. Spectral analysis

We determine the spectral properties using both spectral fitting and the hardness ratios. We extract spectral files for the 11 brighter ($f_{0.2-8\ \mathrm{keV}} > 4\times10^{-14}$ erg cm^{-2} s^{-1}) type-I QSO where the signal to noise ratio is relatively high. Moreover, we calculate the Hardness Ratios (HR) for all sources. In Table 1 we give the extracted source and background counts in the 0.2–8 keV energy band for the 32 QSOs as obtained from the EMLDETECT task in the SAS analysis software.

3.1. The spectra of the brighter sources

We derive the spectral files of the 11 brighter sources by using an extraction radius of 32 arcsec (∼8 pixel). We extract the background spectrum from parts of the image which do not contain any obvious sources. We use the response matrix epn_ff20_sdY9.rmf provided by the *XMM-Newton* calibration page (`http://xmm.vilspa.esa.es`) which takes into account both the single and double events. We finally create auxiliary files at every off-axis angle using the ARFGEN task. The source spectra were grouped to give a minimum number of 15 counts per bin so that Gaussian statistics apply. The spectrum of all the sources was fitted in XSPEC v11. The errors quoted in the spectral analysis with XSPEC correspond to the 90% confidence level. We fit the spectra in the 0.5–8 keV band, using an absorbed power–law model. However, only in one case (source #32) we detect an equivalent neutral hydrogen column density, N_H, significantly greater than the Galactic column of 6×10^{19} cm^{-2} (Dickey & Lockman 1990). In Table 2 we present the spectral fit results. We obtain good fits in most cases. Source #3 presents a bad χ^2 suggesting a complex spectrum (see Fig. 1). In the four brighter cases (sources # 8, 22, 27, 32) we attempt to fit the data using a more complicated model consisting of two power-law components. We obtain a statistically significant improvement only in the case of source #8; $\Delta\chi^2 \approx 9.5$ for an additional parameter which is significant at over the 99% confidence level. The high energy power-law is fixed at $\Gamma = 1.9$ while the soft power-law is $\Gamma = 3.45^{+0.32}_{-0.28}$. The *single* power-law spectrum of this source is also plotted in Fig. 1.

3.2. The hardness ratios

We calculate three hardness ratios using the source counts in the following energy bands $S1$ = 0.2–0.5 keV, $S2$ = 0.5–2 keV, M = 2–4.5 keV and H = 4.5–8 keV. The hardness ratios are defined as $HR1 = (S2-S1)/(S2+S1)$, $HR2 = (M-S2)/(M+S2)$, $HR3 = (H-M)/(H+M)$. The hardness ratios are estimated using the EMLDETECT task in SAS, which corrects both for vignetting and for the light falling outside the detection circle (PSF correction). The hardness ratios are given in Table 3 together with their 1σ uncertainties. The uncertainties are estimated using Poisson statistics and error propagation. Given the energy range of each HR, $HR1$ is more sensitive to the presence of a soft excess component or even low amounts of column density (10^{20} cm^{-2}). $HR2$ is affected by the presence of column densities $\sim10^{21}$ cm^{-2} while $HR3$ values could be

Table 1. The hardness ratios.

Name	No.	z	Source counts $\times 10^2$	Error $\times 10^2$	Background counts $\times 10^2$
RX J105125.4+573050	1	3.40	1.52	0.20	0.54
RX J105144.8+572808	2	3.40	1.64	0.19	0.53
RX J105154.4+573438	3	0.87	6.62	0.34	0.61
RX J105213.3+573222	4	1.87	1.86	0.20	0.59
RX J105224.7+573010	5	1.00	1.60	0.18	0.54
RX J105228.4+573104	6	0.93	1.17	0.18	0.61
RX J105230.3+573914	7	1.44	5.29	0.32	0.62
RX J105239.7+572432	8⋆	1.11	38.7	0.77	0.45
RX J105243.1+571544	9	2.14	3.00	0.26	0.52
RX J105245.7+573748	10	1.68	0.75	0.17	0.69
RX J105247.9+572116	11	0.46	10.3	0.40	0.39
RX J105254.3+572343	12	0.76	4.88	0.28	0.35
RX J105257.1+572507	13	1.52	4.31	0.27	0.41
RX J105259.2+573031	14	1.67	3.73	0.28	0.81
RX J105302.6+573759	15	1.88	3.46	0.27	0.71
RX J105303.9+572925	16	0.78	3.26	0.25	0.75
RX J105306.2+573426	17	2.94	1.45	0.20	0.81
RX J105307.2+571506	18⋆	2.41	1.61	0.21	0.48
RX J105309.4+572822	19	1.56	3.83	0.27	0.71
RX J105312.5+573425	20	1.20	2.70	0.24	0.81
RX J105312.4+572507	21	0.96	1.16	0.17	0.60
RX J105316.8+573552	22⋆	1.2	36.2	0.76	0.75
RX J105322.2+572852	23	2.30	1.38	0.19	0.76
RX J105324.7+572819	24	1.51	1.17	0.19	0.76
RX J105329.2+572104	25	1.14	1.57	0.19	0.46
RX J105331.8+572454	26	1.95	10.4	0.41	0.66
RX J105335.1+572542	27	0.78	26.3	0.65	0.69
RX J105339.7+573105	28	0.58	20.7	0.57	0.70
RX J105344.9+572841	29	1.81	5.15	0.30	0.74
RX J105350.3+572710	30	1.70	4.49	0.29	0.67
RX J105358.5+572925	31	1.84	0.95	0.17	0.64
RX J105421.1+572545	32⋆	0.20	56.1	1.02	0.46

⋆ Radio Loud QSO.

Table 2. Spectral fitting results for the 11 brighter sources.

Name	No.	z	$N_{\rm H}$ $\times 10^{22}$ cm^{-2}	Γ	χ^2/d.o.f
RX J105154.4+573438	3	0.87	$0.^{+0.03}$	$2.41^{+0.26}_{-0.24}$	60.1/34
RX J105230.3+573914	7	1.44	$0.^{+0.08}$	$2.06^{+0.53}_{-0.22}$	14.5/27
RX J105239.7+572432	8⋆	1.11	$0.^{+0.01}$	$2.27^{+0.08}_{-0.08}$	126.6/119
RX J105247.9+572116	11	0.46	$0.^{+0.04}$	$2.39^{+0.26}_{-0.19}$	32.3/40
RX J105316.8+573552	22⋆	1.20	$0.^{+0.01}$	$1.87^{+0.05}_{-0.07}$	120.4/136
RX J105331.8+572454	26	1.95	$0.03^{+0.05}_{-0.03}$	$2.17^{+0.30}_{-0.25}$	51.9/53
RX J105335.1+572542	27	0.78	$0.04^{+0.03}_{-0.03}$	$2.15^{+0.15}_{-0.15}$	96.7/107
RX J105339.7+573105	28	0.58	$0.^{+0.02}$	$2.32^{+0.14}_{-0.09}$	85.0/73
RX J105344.9+572841	29	1.81	$0.^{+0.07}$	$1.93^{+0.42}_{-0.22}$	24.4/29
RX J105350.3+572710	30	1.70	$0.^{+0.08}$	$1.67^{+0.42}_{-0.18}$	21.8/30
RX J105421.1+572545	32⋆	0.20	$0.15^{+0.03}_{-0.02}$	$1.87^{+0.09}_{-0.06}$	261.0/257

⋆ Radio Loud QSO.

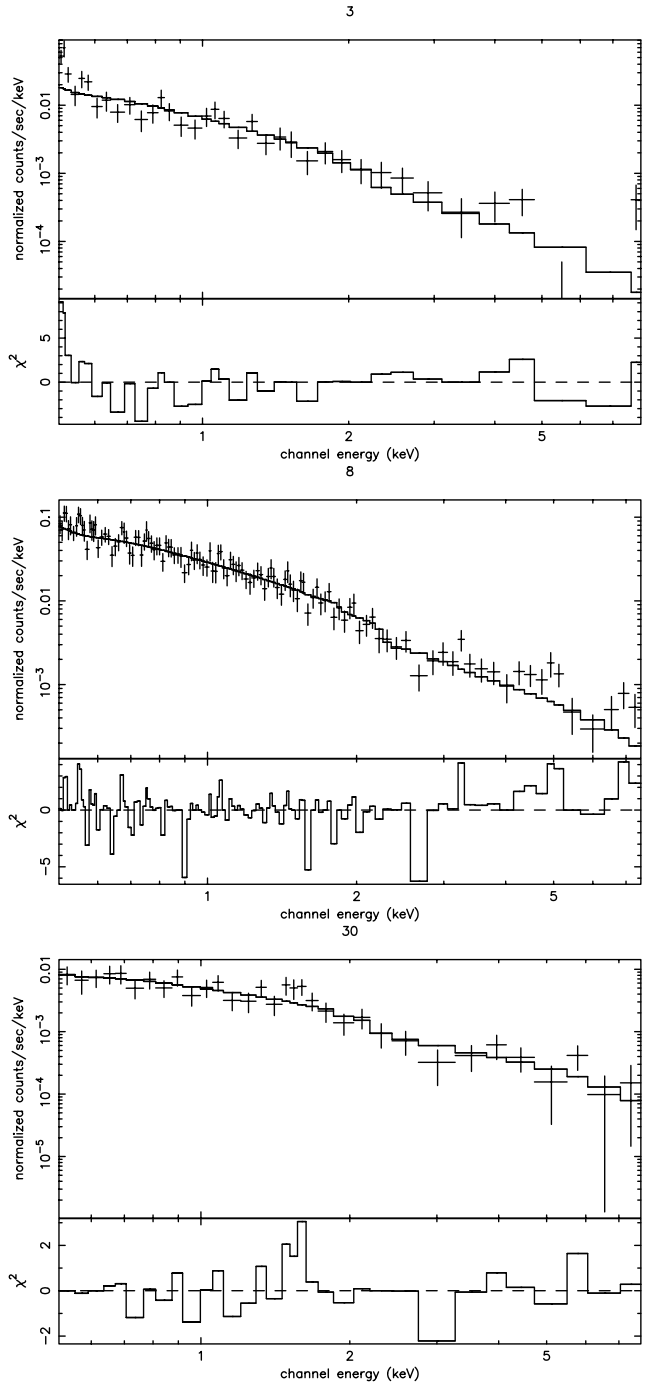

Fig. 1. Power-law fits and χ^2 residuals to the spectra of the sources #3, 8 and 30.

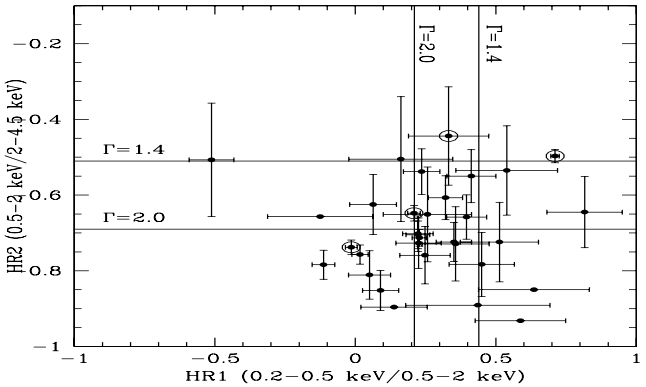

Fig. 2. The *HR*2 (0.5–4.5 keV) as a function of the *HR*1 (0.2–2 keV) hardness ratios for radio-quiet (solid circles) and radio-loud (open circles) QSOs. The solid lines denote power-law spectra with spectral indices of $\Gamma = 2$ and $\Gamma = 1.4$ absorbed by a column density of 6×10^{19} cm^{-2}.

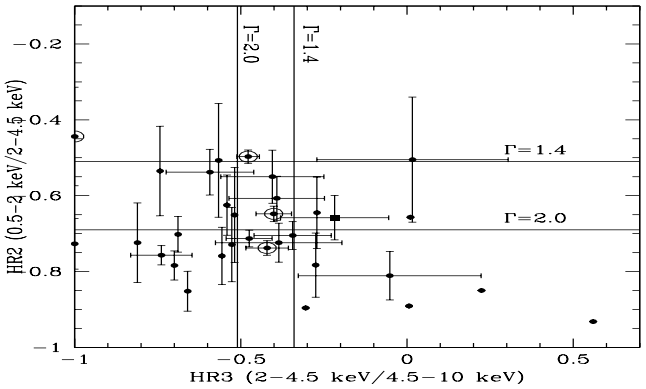

Fig. 3. The *HR*2 (0.5–4.5 keV) as a function of the *HR*3 (2–8 keV) hardness ratios for radio-quiet (solid circles) and radio-loud (open circles) QSOs. The solid lines denote power-law spectra absorbed by a column density of 6×10^{19} cm^{-2}.

sensitive to either a reflection component or to even larger columns (i.e. $>10^{22}$ cm^{-2}).

In Fig. 2 we plot the *HR*2 versus *HR*1 for our 32 sources while in Fig. 3 we plot the *HR*2 versus the *HR*3 hardness ratio. For the sake of clarity, we plot the errors only in the cases where we have at least 15 counts in each energy band. In Fig. 2 we find several sources with a spectrum harder than $HR1 \sim 0.45$ ($\Gamma = 1.4$) in the soft band (#1, 2, 21, 23, 24, 32). These have softer spectra in the hard (2–8 keV) band (see the *HR*3 values, Table 3) and therefore absorption is the most likely explanation for the hard *HR*1 ratios. In the case of the source #32, which is bright enough to allow for spectral fitting, we find that indeed the spectrum is absorbed by an intrinsic column of $\sim 2 \times 10^{21}$ cm^{-2}. The other five sources are located at higher redshifts so that, if the absorption is intrinsic, the *rest-frame* columns are much larger. For example for sources #1 and 2, both located at a redshift of $z \approx 3.4$, the observed hardness ratios translate to columns of $\sim 5 \times 10^{22}$ and $\sim 3 \times 10^{23}$ cm^{-2} respectively, assuming a spectrum with $\Gamma = 2.0$. This is in agreement with earlier findings by Fiore et al. (1999), Akiyama et al. (2000) who first presented evidence for the existence of absorbed broad-line QSOs, using *BeppoSAX* and *ASCA* data respectively. In Fig. 3, there are a few sources with a more complex behaviour. These show marginal evidence (given the large error bars in *HR*3) for spectral hardening at high energies ($HR3 > -0.3$ or $\Gamma < 1.4$) while their soft spectra are steep (cf. Giommi et al. 2000; Barcons et al. 2002). Only one of our sources with a flat hardness ratio at hard energies (*HR*3) is bright enough (#30) to allow us to derive a detailed spectral fit (see Fig. 1 and Table 2). The fit gives a relatively hard spectrum $\Gamma = 1.67^{+0.42}_{-0.18}$, (albeit with large uncertainty). This spectrum is somewhat steeper, but comparable to that derived from the *HR*3 hardness ratio (the 68% upper limit of *HR*3

Table 3. The source list.

Name	No.	z	log(0.2–8 keV flux)[1] ergs s^{-1} cm^{-2}	*HR*1	*HR*2	*HR*3
RX J105125.4+573050	1	3.40	−13.89 ± 0.058	0.513 ± 0.139	−0.724 ± 0.105	−0.811 ± 0.654
RX J105144.8+572808	2	3.40	−13.96 ± 0.052	0.816 ± 0.134	−0.645 ± 0.094	−0.271 ± 0.276
RX J105154.4+573438	3	0.87	−13.33 ± 0.022	0.223 ± 0.054	−0.702 ± 0.046	−0.689 ± 0.167
RX J105213.3+573222	4	1.87	−14.00 ± 0.048	0.450 ± 0.116	−0.783 ± 0.084	−0.275 ± 0.401
RX J105224.7+573010	5	1.00	−14.14 ± 0.050	0.357 ± 0.120	−0.729 ± 0.098	−0.527 ± 0.421
RX J105228.4+573104	6	0.93	−14.26 ± 0.066	0.162 ± 0.185	−0.505 ± 0.165	0.016 ± 0.288
RX J105230.3+573914	7	1.44	−13.35 ± 0.026	0.351 ± 0.063	−0.724 ± 0.051	−0.386 ± 0.190
RX J105239.7+572432	8⋆	1.11	−12.73 ± 0.008	−0.014 ± 0.021	−0.738 ± 0.019	−0.421 ± 0.064
RX J105243.1+571544	9	2.14	−13.51 ± 0.038	0.248 ± 0.089	−0.759 ± 0.075	−0.557 ± 0.420
RX J105245.7+573748	10	1.68	−14.27 ± 0.100	0.436 ± 0.257	−0.891 ± 0.167	0.006 ± 1.286
RX J105247.9+572116	11	0.46	−13.20 ± 0.017	−0.113 ± 0.040	−0.784 ± 0.038	−0.700 ± 0.185
RX J105254.3+572343	12	0.76	−13.60 ± 0.025	0.321 ± 0.061	−0.607 ± 0.058	−0.392 ± 0.144
RX J105257.1+572507	13	1.52	−13.69 ± 0.027	0.089 ± 0.064	−0.852 ± 0.053	−0.660 ± 0.432
RX J105259.2+573031	14	1.67	−13.77 ± 0.032	0.413 ± 0.087	−0.550 ± 0.070	−0.405 ± 0.155
RX J105302.6+573759	15	1.88	−13.57 ± 0.033	0.063 ± 0.083	−0.625 ± 0.079	−0.542 ± 0.243
RX J105303.9+572925	16	0.78	−13.83 ± 0.033	0.225 ± 0.081	−0.727 ± 0.066	−1.000 ± 0.264
RX J105306.2+573426	17	2.94	−14.01 ± 0.061	0.257 ± 0.157	−0.651 ± 0.125	−0.519 ± 0.433
RX J105307.2+571506	18⋆	2.41	−13.73 ± 0.059	0.332 ± 0.143	−0.444 ± 0.130	−1.00 ± 0.408
RX J105309.4+572822	19	1.56	−13.74 ± 0.031	0.050 ± 0.075	−0.811 ± 0.063	−0.052 ± 0.276
RX J105312.5+573425	20	1.20	−13.78 ± 0.039	−0.512 ± 0.079	−0.507 ± 0.015	−0.567 ± 0.386
RX J105312.4+572507	21	0.96	−14.22 ± 0.067	0.588 ± 0.161	−0.932 ± 0.107	0.560 ± 0.605
RXJ105316.8+573552	22⋆	1.20	−12.60 ± 0.009	0.209 ± 0.022	−0.648 ± 0.021	−0.401 ± 0.053
RX J105322.2+572852	23	2.30	−14.13 ± 0.062	0.539 ± 0.181	−0.535 ± 0.118	−0.743 ± 0.333
RX J105324.7+572819	24	1.51	−14.19 ± 0.070	0.636 ± 0.197	−0.850 ± 0.110	0.224 ± 0.473
RX J105329.2+572104	25	1.14	−13.91 ± 0.053	0.138 ± 0.119	−0.896 ± 0.104	−0.305 ± 1.171
RX J105331.8+572454	26	1.95	−13.18 ± 0.017	0.223 ± 0.042	−0.705 ± 0.037	−0.344 ± 0.116
RX J105335.1+572542	27	0.78	−12.77 ± 0.010	0.228 ± 0.025	−0.713 ± 0.022	−0.475 ± 0.069
RX J105339.7+573105	28	0.58	−12.86 ± 0.012	0.016 ± 0.028	−0.757 ± 0.025	−0.739 ± 0.092
RX J105344.9+572841	29	1.81	−13.44 ± 0.025	0.236 ± 0.065	−0.538 ± 0.060	−0.593 ± 0.132
RX J105350.3+572710	30	1.70	−13.47 ± 0.028	0.396 ± 0.071	−0.658 ± 0.058	−0.218 ± 0.163
RX J105358.5+572925	31	1.84	−14.10 ± 0.081	−0.125 ± 0.187	−0.657 ± 0.215	−0.010 ± 0.584
RX J105421.1+572545	32⋆	0.20	−12.19 ± 0.007	0.711 ± 0.015	−0.497 ± 0.018	−0.478 ± 0.034

⋆ Radio loud.
[1] Assuming a power-law model with $\Gamma = 2$.

corresponds to $\Gamma \approx 1.5$) and in much better agreement with the spectrum derived on the basis of the *HR*2 hardness ratio (which is consistent with $\Gamma = 2$). We therefore believe that there is no conclusive evidence in our data for the presence of a population of *soft X-ray selected* QSOs with intrinsically flat spectra at hard energies.

Next, we investigate whether there is a correlation between the hardness ratio and the X-ray flux. Hasinger et al. (1993) and Della Ceca et al. (1999), presented evidence for such a relation, in the sense that the photon index becomes harder with decreasing flux, using *ASCA* and *ROSAT* data. However, their samples contain all X-ray sources, not just QSOs in contrast to our sample. We divide the data into three flux bins and we calculate the mean value of HR. The mean is calculated by averaging the individual hardness ratios in each flux bin (no weights for the individual HR errors are applied). The advantage of estimating the mean HR value in the way above – as compared to adding up the counts in each bin – is that the much larger errors reflect the intrinsic spectral dispersion of the QSO population. We exclude the brighter (and nearest) source of our sample (# 32) which is a relatively absorbed ($N_{\rm H} \sim 2{\times}10^{21}$) QSO at $z = 0.2$. In Table 4 we present the HR values for each flux bin. In Fig. 4 we plot the individual HR values (*HR*1, *HR*2, *HR*3) as a function of flux together with the mean HR values for the three flux bins. Each bin contains roughly the same number of sources while the flux corresponds to the middle of the bin. There is no statistically significant correlation of any of the HR with flux. Moreover, we explore any possible dependence of the HR on redshift. We derive the mean values of HR in three redshift bins (Table 5 and Fig. 5). We choose the groups so that each one contains roughly the same number of sources. We find no dependence of any of the HR on redshift. The lack

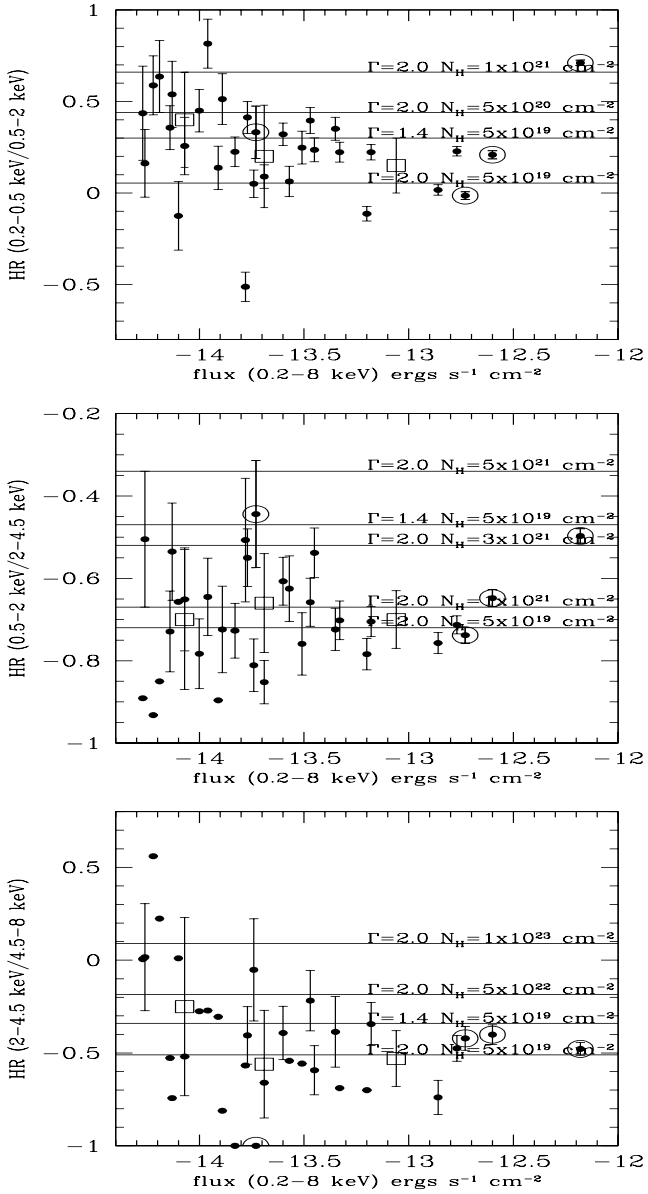

Fig. 4. HR values as a function of the 0.2–8 keV flux: *HR*1 (upper panel), *HR*2 (middle panel) *HR*3 (lower panel). The solid and open circles denote the radio-loud and radio-quiet QSOs respectively. Errors are plotted only for sources having at least 15 counts in each band. The open boxes represent the mean HR values.

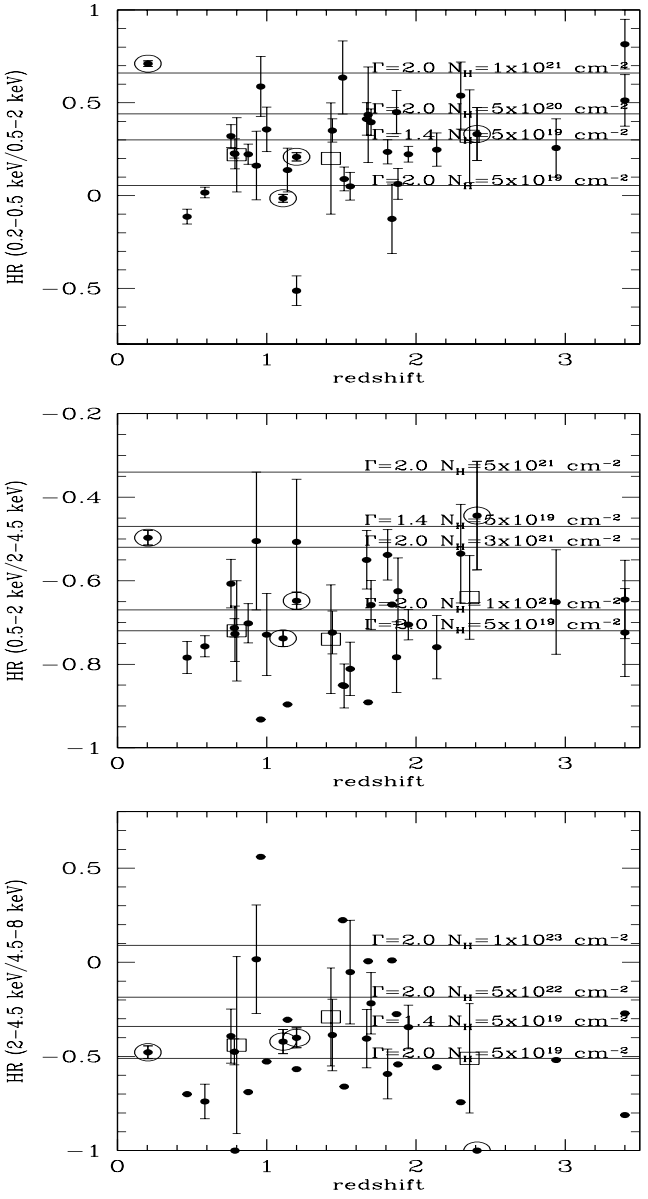

Fig. 5. HR values of type I QSOs as a function of redshift: *HR*1 values (upper), *HR*2 (middle), *HR*3 (lower panel). The solid and open circles denote the radio-loud and radio-quiet QSOs respectively. Errors are plotted only for sources having at least 15 counts in each band. The open boxes represent the mean value.

of relation between *HR*1 and redshift suggests that the intrinsic column density is not a function of redshift *or* luminosity (as there is a strong correlation between redshift and luminosity). The lack of correlation between *HR*1 and redshift also comes in contradiction to the results of Schartel et al. (1996) and Blair et al. (2000). However, the *number* statistics of our sample are still very limited (∼10 sources per redshift bin) to allow us to draw definitive conclusions. Finally, the fact that *HR*3 does not get harder with increasing redshift suggests that the strengths of any reflection components at high energies (>10 keV) must be small.

We also compare the obtained *HR*1 values with that presented by Lehmann et al. (2001) using *ROSAT* data. Note that Lehmann et al. (2001) have calculated the HR using data in slightly different energy bands, namely 0.1–0.4 keV and 0.4–2 keV. In order to convert the *ROSAT* and *XMM-Newton* HR to photon index we assume a power-law spectrum of $\Gamma = 2$ absorbed by the Galactic column density 6×10^{19} cm^{-2}. In Fig. 6 we plot the *XMM-Newton* photon index versus *ROSAT* photon index for our sources. There is very good agreement between the *ROSAT* and *XMM-Newton HR*1 values in most cases.

3.3. The average QSO spectrum

We finally derive the average QSO spectrum in the 0.5–8 keV band by co-adding the photons from all 32 QSOs, in the observer's frame. The vignetting and PSF

Table 4. Mean HR values for three flux bins.

mean flux (0.2–8 keV) ergs s^{-1} cm^{-2}	[1]No.	*HR*1	*HR*2	*HR*3
8.70×10^{-14}	9	0.15 ± 0.15	−0.70 ± 0.07	−0.53 ± 0.15
2.04×10^{-14}	11	0.20 ± 0.28	−0.66 ± 0.12	−0.56 ± 0.29
0.85×10^{-14}	11	0.40 ± 0.26	−0.70 ± 0.17	−0.25 ± 0.48

[1] Number of stacked AGN.

Table 5. Mean HR values for three redshift bins.

mean *z*	[1]No.	*HR*1	*HR*2	*HR*3
0.80	9	0.22 ± 0.20	–0.72 ± 0.12	–0.44 ± 0.47
1.43	11	0.20 ± 0.30	–0.74 ± 0.13	–0.29 ± 0.26
2.36	11	0.32 ± 0.25	–0.64 ± 0.10	–0.51 ± 0.29

[1] Number of QSOs in the bin.

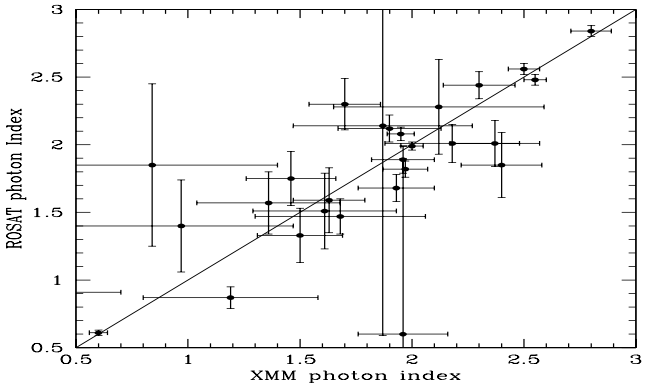

Fig. 6. The *ROSAT* versus the *XMM-Newton* spectrum. The *ROSAT* photon index is derived from the 0.1–2 keV hardness ratio while the *XMM-Newton* photon index from the 0.2–2 keV hardness ratio.

corrections were applied by creating 32 auxiliary files with the SAS task ARFGEN and then co-adding them using the ADDARF task of FTOOLS. The spectral fit to a power-law model yields $\Gamma = 1.86^{+0.02}_{-0.02}$ with column density $N_{\rm H} \approx 0^{+1} \times 10^{20}$ cm^{-2} ($\chi^2 = 569.6/524$). Although the fit is very good, we tried to fit separately the hard (2–8 keV) and soft (0.5–2 keV) energies in order to check whether there is any hint for a more complex model. We find very good agreement between the two power-laws with $\Gamma_{\rm soft} = 1.88^{+0.05}_{-0.04}$ and $\Gamma_{\rm hard} = 1.94^{+0.07}_{-0.12}$. The average spectrum of the 32 QSOs is shown in Fig. 7; there we also plot the best fit model and the χ^2 residuals. The derived mean "typical" QSO spectrum is significantly steeper than the spectrum of the X-ray background in both soft and hard energies. Indeed, results from all X-ray missions have demonstrated that the spectrum of the X-ray background is $\Gamma = 1.4$–1.5 in the 1–10 keV band (Gendreau et al. 1995; Vecchi et al. 1999). As the above average spectrum is dominated by our 11 bright sources, we have derived separately the spectrum for the 21 faint sources. Again we find a steep spectrum ($\Gamma = 1.94^{+0.10}_{-0.10}$ with $\chi^2 = 259.4/224$) consistent with the total spectrum. Hence soft X-ray selected, broad-line AGN with obscured spectra do not contribute significantly to the

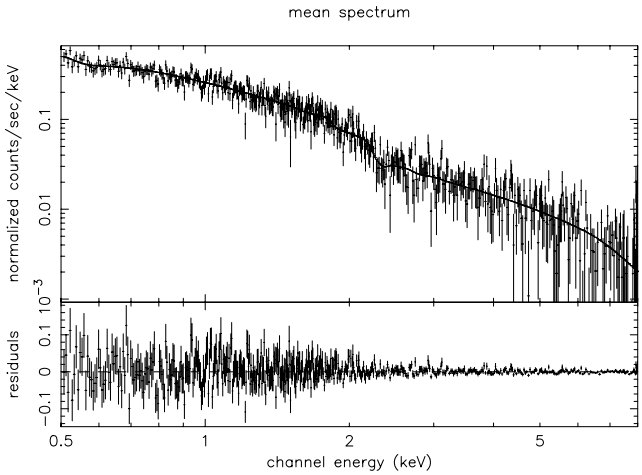

Fig. 7. The average spectrum of the 32 QSOs plotted with the best-fit power-law model and the χ^2 residuals.

total QSO flux in this field. Page (1998) also finds that the average *ASCA* spectrum of the soft X-ray selected QSOs from the RIXOS sample is steep ($\Gamma \sim 1.8$). These results come in apparent contradiction to the findings of Pappa et al. (2001) and Barcons et al. (2002) who find spectral hardening in the average QSO spectrum. However, we note that our sample contains only soft X-ray selected QSOs in contrast to the surveys of Pappa et al. (2001) and Barcons et al. (2002). Soft X-ray selected samples preferentially select soft or unabsorbed sources possibly explaining the apparent discrepancy.

4. Summary

We present the spectral analysis of 32 type-1 (broad-line) QSOs in the Lockman Hole. These faint QSOs ($f_{0.2-8\ \rm keV} > 5 \times 10^{-15}$ erg cm^{-2} s^{-1}) contribute an appreciable fraction (∼50%) of the soft X-ray background. For the 11 bright sources, where good photon statistics are available, we derive the individual spectra. Most of these 11 bright QSOs present the canonical AGN spectrum ($\Gamma \sim 1.9$) or steeper with little or no significant absorption above the Galactic value. These findings are in excellent agreement with previous *ASCA* results on (predominantly optically selected) QSOs eg Reeves & Turner (2000). The HR analysis shows evidence for QSOs with large absorbing columns (up to 10^{23} cm^{-2} in the QSO's rest-frame). This finding is in agreement with previous results by Fiore et al. (1999) and Akiyama et al. (1999). There is no conclusive evidence from our individual spectra or hardness ratios for spectral hardening at high energies.

Although there is evidence that the spectrum of a few faint QSOs presents large absorbing columns, the average spectrum of all 32 QSOs has the canonical value of $\Gamma \sim 1.9$. This is much steeper than the spectrum of the X-ray background in the 1–10 keV band. This is also significantly steeper than the average QSO spectrum found in hard X-ray selected QSO samples (Pappa et al. 2001; Barcons et al. 2002). The accumulation of further, deeper *XMM-Newton* data as well as future observations with high effective area missions such as *Constellation-X* and *XEUS* will allow us to shed more light on the spectral properties of moderate to high redshift QSOs.

Acknowledgements. We are grateful to the referee Dr. Belinda Wilkes for her numerous corrections and suggestions. This work has been supported by a Greek-Spanish bilateral Scientific Agreement grant under the title "Search for Obscured AGN with XMM". Partial financial support for XB was provided by the Spanish Ministry of Science and Technology under project AYA2000-1690. This work is based on data obtained from the *XMM-Newton* public data archive.

References

Akiyama, M., Ohta, K., Yamada, T., et al. 2000, ApJ, 532, 700
Barcons, X., Carrera, F. J., Watson, M. G., et al. 2002, A&A, 382, 522
Blair, A. J., Stewart, G. C., Georgantopoulos, I., et al. 2000, MNRAS, 314, 138
Comastri, A., Setti, G., Zamorani, G., & Hasinger, G. 1995, A&A, 296, 1
della Ceca, R., Castelli, G., Braito, V., Cagnoni, I., & Maccacaro, T. 1999, ApJ, 524, 674
de Ruiter, H. R., Zamorani, G., Parma, P., et al. 1997, A&A, 319, 7
Dickey, J. M., & Lockman, F. J. 1990, ARA&A, 28, 215
Fiore, F., La Franca, F., Giommi, P., et al. 1999, MNRAS, 306, L55
Gendreau, K. C., Mushotzky, R. F., Fabian, A., et al. 1995, PASJ, 47, L5
Giommi, P., Perri, M., & Fiore, F. 2000, A&A, 362, 799
Hasinger, G., Burg, R., Giacconi, R., et al. 1993, A&A, 275, 1
Hasinger, G., Altieri, B., Arnaud, M., et al. 2001, A&A, 365, L45
Iwasawa, K., Fabian, A. C., & Nandra, K. 1999, MNRAS, 307, 611
Kellermann, K. I., Sramek, R. A., Schmidt, M., Shaffer, D. B., & Green, R. 1989, AJ, 108, 1163
Lawson, A. J., & Turner, M. J. L. 1997, MNRAS, 288, 920
Lehmann, I., Hasinger, G., Schmidt, R., et al. 2001, A&A, 371, 833
Mainieri, V., Bergeron, J., Hasinger, G., et al. 2002, A&A, 393, 425
Miyaji, T., Ishisaki, Y., Ogasaka, Y., et al. 1998, A&A, 334, L13
Mushotzky, R. F., Done, C., & Pounds, K. A. 1993, ARA&A, 31, 717
Page, M. J. 1998, MNRAS, 298, 537
Pappa, A., Stewart, G. C., Georgantopoulos, I., et al. 2001, MNRAS, 327, 499
Reeves, J., & Turner, M. 2000, MNRAS, 316, 234
Schartel, N., Walter, R., Fink, H. H., & Trümper, J. 1996, MNRAS, 283, 1015
Schmidt, M., Hasinger, G., Gunn, J., et al. 1998, A&A, 329, 495
Strüder, L., Briel, U., Dennerl, K., et al. 2001, A&A, 365, 18
Vecchi, A., Molendi, S., Guainazzi, M., Fiore, F., & Parmar, A. N. 1999, A&A, 349, L73